# Preparation and chemical mechanical polishing performance of $CeO_2/CeF_3$ composite powders

*Chuan Zhou, Dachuan Zhu* ✉

*College of Material Science and Engineering, Sichuan University, Chengdu 610065, People's Republic of China*
✉ *E-mail: zhudachuan@scu.edu.cn*

Published in Micro & Nano Letters; Received on 3rd May 2017; Revised on 19th July 2017; Accepted on 1st September 2017

This work reported a simple route for preparing $CeO_2/CeF_3$ composite powders. Cerium nitrate hexahydrate, oxalic acid dihydrate and ammonium fluoride were milled and subsequently calcined to obtain the composite powders. X-ray diffractometer, field emission scanning electron microscope, transmission electron microscopy, zeta potential tester, and polishing test were utilised to characterise those products and study the effect of doped fluorine amount on their physicochemical characteristics and chemical mechanical polishing properties. The results show that incorporation of 7 wt% fluorine into the starting materials can change the particle morphology from large sheet for pure $CeO_2$ into uniform spherical particles with size of 30–50 nm. The composite powder with 7 wt% fluorine exhibits great suspension stability and relatively high material removal rate. Meanwhile, this slurry facilitates obtaining smoother surface after polishing, which may be related to the changes of particle morphology and decrease in overall hardness of abrasives.

**1. Introduction:** Chemical mechanical polishing (CMP) is extensively applied in the industry of semiconductor and other fields for global planarisation, such as production of integrated circuit photomasks, computer hard disks, liquid crystal display glass, ultraprecise ceramics, and high-precise valves [1, 2]. Differing from traditional polishing technologies, CMP technology combines the mechanical effect and chemical effect to remove materials [2–4], resulting in higher polishing efficiency and better surface fineness. As a key factor of CMP technology, the CMP slurry, especially the compositions of the abrasives, has a strong impact on the CMP process.

Compared with the traditional polishing materials, such as $Fe_2O_3$, $Al_2O_3$, $SiO_2$, and $ZrO_2$, $CeO_2$ is recognised to be one of the most promising CMP materials, due to the advantages of high polishing rate, long service life, and low pollution [5, 6]. Hence researches on the polishing performance of ceria slurry have sprung up in recent years [5, 7, 8]. Nonetheless, the progressively lifted demand of surface precision in the polishing field has tremendously increased the requirement of synthesis of new polishing powders, which need to possess proper particle size and narrow size distribution as well as other excellent features so as to fulfil the fabrication of efficiently damage-free surfaces. Herein, two technical routes are alternative: one is accurate control of the size, size distribution and morphology of ceria powders, the other is composting with other kinds of materials. The latter can effectively improve the CMP performance of ceria powders [9], whereupon researches on various ceria-based composite materials have grown by leaps and bounds. For example, Chen *et al.* [10] synthesised core–shell structured polystyrene@ceria (PS@$CeO_2$) nanocomposites. Masato *et al.* [11] prepared a new Ce-containing ternary mixed oxide ($CeTi_2O_6$) via the Pechini polymerisable complex method. Lei *et al.* [12] synthesised silica/ceria nanocomposite abrasives via homogeneous precipitation. Compared with traditional single abrasives, these composite polishing abrasives exhibit higher material removal rate (MRR), better surface planarisation and less scratch on the substrate surface. However, these fabrication technologies of composite powders involve additional synthesis procedures of the incorporated materials as well as complicated procedures to form composite structures, which may increase the cost and lower efficiency in large-scale production. By contrast, though $CeF_3$ has a lower hardness than $CeO_2$, it is a very stable material in high-temperature field [9], therefore the fabrication of $CeO_2/CeF_3$ composite powders will be very interesting and significant. Zhang and co-workers [9] prepared $CeO_2/CeF_3$ composite powders via a wet chemical method, in which hydrated cerium carbonate ($Ce_2(CO_3)_3{\cdot}H_2O$) and fluorine hydride were employed as cerium and fluorine sources, respectively. Yet the morphology of their products is uneven microsized grape-like shape, resulting in some scratches remaining on the quartz surfaces after polishing. Moreover, the evolutional process of particle morphologies and related mechanism were not studied in depth. Therefore, study on nanosized $CeO_2/CeF_3$ composite powders is still a challenging issue with a great significance.

In this work, we reported a simple synthesis strategy for $CeO_2/CeF_3$ composite powders through mechanochemical reaction followed by a calcination procedure. Cerium nitrate hexahydrate, oxalic acid dihydrate, and ammonium fluoride were applied as starting materials. Then a series of methods, including X-ray diffractometer, field emission scanning electron microscope (FESEM), transmission electron microscopy (TEM), zeta potential tester, and CMP test, were utilised to characterise the as-synthesised products and study the effect of doped fluorine amount on their physicochemical characteristics and CMP properties. Finally related mechanism was studied.

## 2. Experimental methods

2.1. Preparation: All chemicals and reagents used in this work were of analytical purity from Kelon Chemical Reagents Company, China. In a typical procedure, a certain amount of cerium (III) nitrate hexahydrate [$Ce(NO_3)_3{\cdot}6H_2O$] and oxalic acid dihydrate ($H_2C_2O_4{\cdot}2H_2O$) as well as the desired amount of ammonium fluoride ($NH_4F$) (fluoride doping content = 0, 3, 5, 7, or 9 wt%) were put into a 250 ml agate jar. Then mechanochemical reaction was carried out on a QM-3SP2 planetary ball-milling machine (Nanda Instruments, China) at ambient temperature, using a ball to powder mass ratio of 10 : 1 and a milling speed of 300 rpm. A small amount of anhydrous ethanol was added into the reaction as lubricant. When milling finished, the obtained products were calcined at 400°C after being washed by deionised water and ethanol three times and dried in an oven at 60°C for several hours. Finally, the all as-calcined powder was slightly milled in an agate mortar to obtain the final product.

2.2. Characterisation: X-ray diffraction (XRD) analysis of the as-prepared powders was performed on a PANalytical Empyrean X-ray diffractometer with Cu target. The morphology and particle

size of the products were observed by use of a JEOL JSM 7500F FESEM and a JEM-100CX TEM. The surface charge of particles in terms of zeta potential was measured using a Malvern Zetasizer ZEN3690 instrument, here the concentration of solution for measurement was fixed to 0.02 wt% and its pH was not adjusted. Polishing experiment was performed with a conventional optical glass slice about 3 × 3 cm on a DMP 3A10 polishing machine (HEBAU Electromechanical, China). The polishing conditions were set as follows: down force 30 N, rotation speed of polishing pad 100 rpm, polishing time 60 min, slurry concentration 1 wt%, dispersant water, and feeding rate of the slurry 20 ml/min. MRR, nm/min was calculated as follows:

$$\mathrm{MRR} = \frac{\Delta m}{\rho \cdot S \cdot t} \tag{1}$$

$\Delta m$ in (1) is the difference of mass of glass between before and after polishing, $\rho$ is the density of glass, $S$ is the polished surface area, and $t$ is the polishing time. The polishing test of every different composite powder was repeated three times and three pieces of glass were used in a repetition. The MRR value was obtained by averaging. Finally, the fineness of the glass surface before and after polishing was observed via a CMM-30E metallographic microscope (Chfang Optics, China) assisted with a SJ-210 surface roughness tester (Mitutoyo, Japan).

## 3. Results and discussion

3.1. XRD analysis: Fig. 1 presents the XRD patterns of the as-prepared pure ceria and $CeO_2/CeF_3$ composite powders with different fluorine incorporation contents. The trace of sample without fluorine incorporation can be indexed to the typical cubic fluorite structure of cerium dioxide (fcc, space group: Fm3m, JCPDS Card No. 43-1002). All ceria's typical diffraction peaks in the composite powder samples (3, 5, 7, and 9%) match well with those of the pure cerium dioxide sample (0%). Once enough $NH_4F$ was added into the solid-phase reactions, the typical diffraction peaks corresponding to $CeF_3$ phase appear in the XRD patterns, indicating that fluorine was successfully doped into $CeO_2$ powders in the form of $CeF_3$. Furthermore, it is noteworthy that with the doped fluorine content increasing, the peak intensity corresponding to $CeF_3$ becomes stronger while the peak intensity corresponding to $CeO_2$ decreases gradually, demonstrating the content increase of $CeF_3$ in the composite powders. Apart from

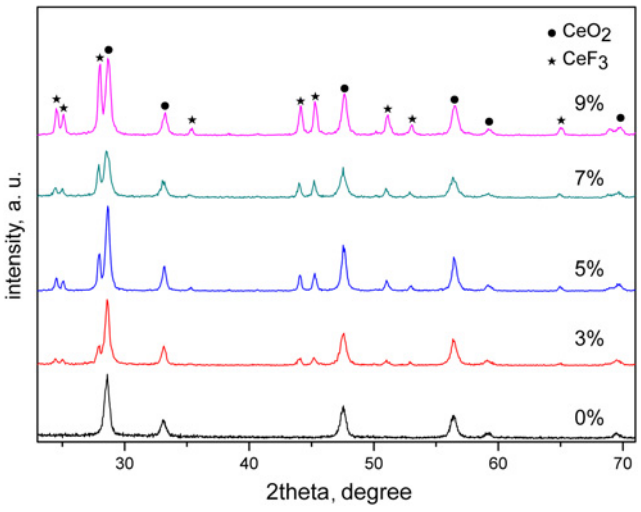


**Fig. 1** *XRD patterns of the pure ceria and the $CeO_2/CeF_3$ composite powders generated from different contents of fluorine being added into the reaction*

$CeF_3$ and $CeO_2$, no other phase can be observed in all measured XRD patterns.

3.2. FESEM analysis: Fig. 2 shows the FESEM images of samples with different incorporation amount of fluorine in the milling process and TEM image of sample with 7 wt% fluorine being added. Obviously, particle size and morphology of these samples change significantly with different contents of fluorine being added into the reaction. Fig. 2*a* shows the morphology and particle size of the pure $CeO_2$ powders generated from the typical solid-phase mechanochemical reaction. It can be seen that the pure $CeO_2$ particles possess morphology of thick irregular sheets and have a rather big and uneven size (0.3–1 μm). The sample in Fig. 2*b* is composed of mostly big sheets with a few fine granular particles; while some big crystal sheets have been broken. The sheet structures in Fig. 2*c* become smaller and less compared to that in Fig. 2*b*, and the fine particles become the most. When the doped fluorine content reaches 7%, as shown in Fig. 2*d*, there are not crystal sheets any more, all particles become uniform (30–50 nm) spherical granules. Furthermore, as the doped fluorine content increases to 9%, partial agglomeration emerges, leading to again appearance of pieces of particles. Fig. 2*f* is the TEM image of the sample with 7% fluorine being added, it shows that most of the particles are spheroidal and a few are irregular polyhedrons. Their size centralises in the range of 30–50 nm as same as their FESEM image (Fig. 2*d*) shows.

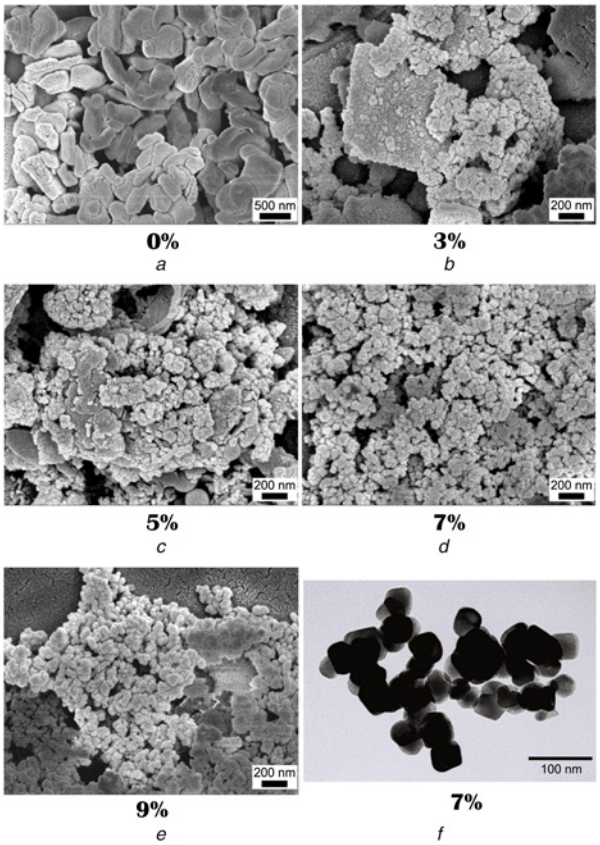


**Fig. 2** *FESEM images and TEM image of samples with different content of fluorine being added*
*a* FESEM image of the 0% product
*b* FESEM image of the 3% product
*c* FESEM image of the 5% product
*d* FESEM image of the 7% product
*e* FESEM image of the 9% product
*f* TEM image of the 7% product




doi: 10.1049/mnl.2017.0303

3.3. Zeta potential analysis: The effect of doping fluorine quantity on zeta potential of the final products is presented in Fig. 3. The results show that all data measured are positive potential, which can be ascribed to the unadjusted pH of the measured slurry. In detail, the pure ceria powders show the maximum zeta potential of +42.2 mV. In this case, the particle morphology is large sheet. Microcosmic force interaction between particles is dominated by gravity, so it is hard for these particles to congeal spontaneously. When fluorine is doped into the reaction, the zeta potential decreases slightly and then stays stable until the doping fluorine contents exceed 7%, indicating that these polishing slurries have great dispersion stability as evidenced by the high zeta potential value of around +35 mV. When doped fluorine content reaches 9%, the zeta potential decreases steeply from 35.8 mV for the fluorine doping content of 7% to 21.8 mV, demonstrating that this slurry has instability and may congeal spontaneously.

3.4. CMP test: The effect of fluorine doping quantity on MRRs of the composite powders is presented in Fig. 4. Obviously, the MRR reaches its maximum value at the fluorine doping content of 5%, and then sharply decreases. According to modern knowledge, the CMP process of cerium-based polishing slurries involves two effects: the physical effect (mechanical cutting) and the chemical effect (formation and breakage of the Ce–O–Si bond) [2, 13, 14]. We believe the results in Fig. 4 are the consequence of competition between the physical effect and chemical effect. When the fluorine doping content is relatively low, as shown in Figs. 2*a* and *b*, the morphology of polishing abrasives is uneven big sheet with poignant edges, which could enhance the mechanical cutting effect. While, the concentration of all used CMP slurries is fixed to 1 wt%. Here the size and size distribution of abrasives are large, the effective abrasive number in unit slurry volume is small. That is, the mechanical cutting effect is dominant in the CMP process. Together, the two factors account for the left shoulder shown in Fig. 4.

On the contrary, when the fluorine doping content is relatively high, the morphology of polishing abrasives is even nanosized spherical granule, which may weaken the mechanical effect to some degree. However, here the size and size distribution of abrasives are small and narrow, the effective abrasive number in unit slurry volume is large.

Thus the polishing process is dominated by the chemical effect, resulting in the right shoulder in Fig. 4. Finally, when the fluorine doping content lies at the middle level of 5%, as shown in Fig. 2*c*, the polishing abrasives are composed of both large sheets and ultrafine spherical granules, the physical effect and chemical effect described above can intimately collaborate, yielding the maximum surface removal rate.

The surface fineness of glass before and after polished by the as-prepared powders with different fluorine doping contents is shown in Fig. 5 and Table 1. Ra and RMS in Table 1 describe the surface roughness. Ra is the arithmetical mean deviation of the profile obtained by surface roughness tester, and RMS is the

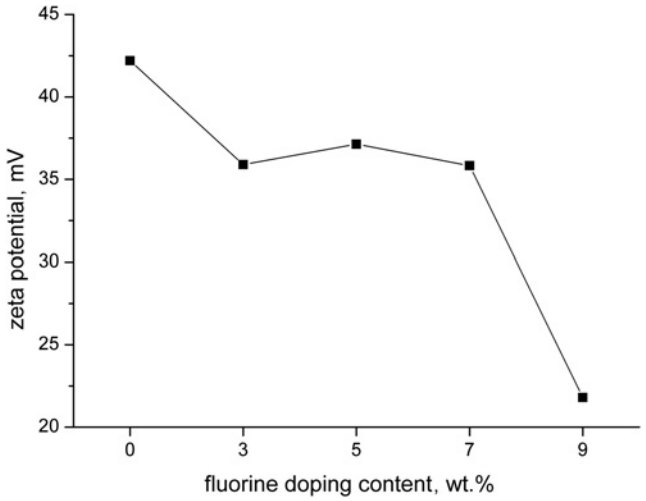


**Fig. 3** *Zeta potential of samples doped with different contents of fluorine*

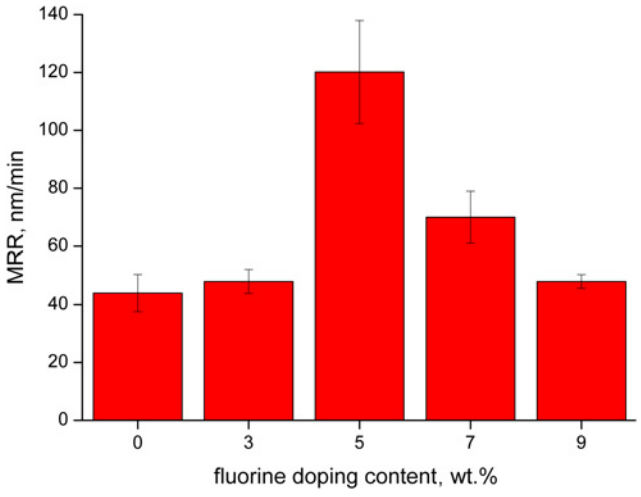


**Fig. 4** *MRRs for samples with different fluorine doping contents*

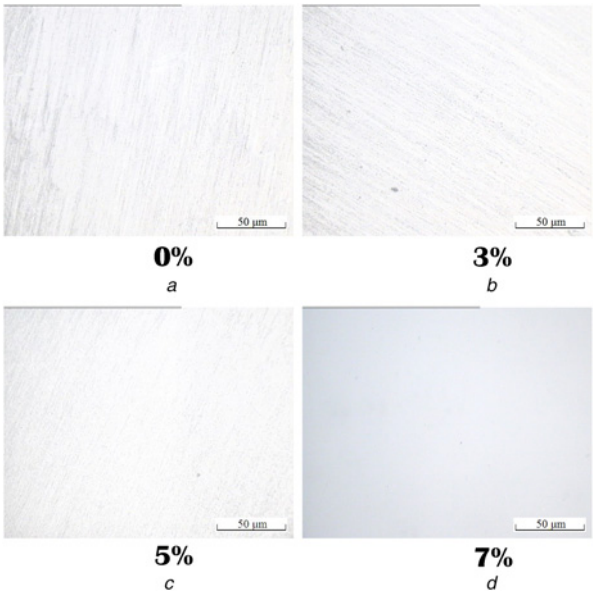


**Fig. 5** *Surface fineness images of glass obtained by metallographic microscope versus fluorine doping contents*

**Table 1** Surface roughness of glass before and after polished by the as-prepared powders with different fluorine doping contents

| Items | Ra, nm | RMS, nm |
|---|---|---|
| before polishing | 8.9 ± 0.4 | 11.3 ± 0.2 |
| after polishing, 0% | 7.1 ± 0.3 | 9.5 ± 0.4 |
| after polishing, 3% | 5.3 ± 0.2 | 6.3 ± 0.2 |
| after polishing, 5% | 4.4 ± 0.3 | 5.1 ± 0.3 |
| after polishing, 7% | 2.1 ± 0.5 | 2.7 ± 0.4 |
| after polishing, 9% | 2.2 ± 0.4 | 2.9 ± 0.4 |

root mean square deviation of the profile. The evaluation length of surface profile is 500 μm. We can see from Table 1 that the original surface of glass before polishing is rather rough. After polished by the pure ceria (0%) powders, the value of Ra decreases slightly, as evidenced by its metallographic image (see Fig. 5*a*), in which there are a lot of thick scratches and obvious overall unevenness. With the increase of doped fluorine contents in the composite polishing powders, the roughness of polished surface gradually decreases meanwhile the scratches in metallographic images become more slender. When the fluorine doping content reaches 7%, as shown in Fig. 5*d*, a smooth surface with a Ra value of 2.1 nm is obtained. Hereafter further augment of fluorine doping contents will lead to a slight rebound of roughness. It is generally known that the abrasive size and morphology have great influence on the fineness of polished surface. We believe there are three major factors contributing to the results described above. Firstly, the Mohs harnesses of $CeO_2$ and $CeF_3$ is 6 and 4.5, respectively, thus incorporation of proper amount fluorine into the products can decrease the overall hardness of the polishing powders, which benefits the fabrication of damage-free surfaces. Secondly, on the basis of keeping great dispersion stability of polishing slurry, incorporation of proper amount fluorine into the products changes the morphology of products into nanosized spherical shape. Similar to the description upper, smaller particle size results in larger effective abrasive number in unit slurry volume. When the polishing pressure is fixed, more abrasives in unit volume give rise to smaller force every abrasive need to bear [15], remaining shallower scratches on the substrate surface. Finally, apart from the slide of abrasives on the polished surface, rolling is another important movement form of abrasives. Compared with other shape, spherical granules can roll easily, so as to obtain smoother surface.

3.5. Discussion: To substantially understand how fluorine affects the particle size and morphology of $CeO_2$ synthesised via solid-phase mechanochemical reaction, the milling reaction was carried out for different time (0.5, 1, 1.5, and 2 h). Fig. 6 shows the FESEM images of precursors obtained after different reaction time without and with (7%) fluorine incorporation. In detail, precursors with none fluorine being added, as shown in Figs. 6*a* and *b*, are composed of almost big uneven (both in size and morphology) crystal sheets with smooth surfaces. The particle morphology shows no obvious change under mechanochemical effect and granules grow larger though milling lasts longer time. Figs. 6*c–f* show the FESEM images of precursors obtained after different reaction time with 7% fluorine being added into the reactions. When reaction time is <1 h, the precursors still mostly consist of big crystal sheets, as shown in Figs. 6*c* and *d*, but some nanosized small granules appear. We conclude they are $CeF_3$ particles formed earlier in the reactions. Because $F^-$ ions have a stronger electronegativity than $(C_2O_4)^{2-}$ ions, part of $F^-$ anions will combine with $Ce^{3+}$ ions first, forming $CeF_3$ particles. As a result, smooth $Ce_2(C_2O_4)_3$ sheets with $CeF_3$ particles attaching on their surfaces are obtained. Crystal sheets in Fig. 6*d* become larger and more regular in shape than those in Fig. 6*c*; meanwhile their surfaces become rougher. As shown in Fig. 6*d*, there are small spherical protuberances forming on the surfaces of crystal sheets when reaction time reaches 1 h, and some crystal sheets have been crushed under the coefficient effect of both ammonium fluoride and mechanical forces. When mechanochemical reaction lasts for 1.5 h, as shown in Fig. 6*e*, all crystal sheets are crushed into smaller pieces. As a result, small spherical protuberances on the surfaces of crystal sheets are dominant. However, we are still able to see the trace of sheet structure. After 2-hour reaction, there are only fine particles, those original crystal sheets disappear without any traces.

Fig. 7 gives the XRD patterns of precursors obtained after different reaction time with 7% fluorine incorporation. It is very clear that peaks corresponding to $CeF_3$ phase are dominated in the precursors,

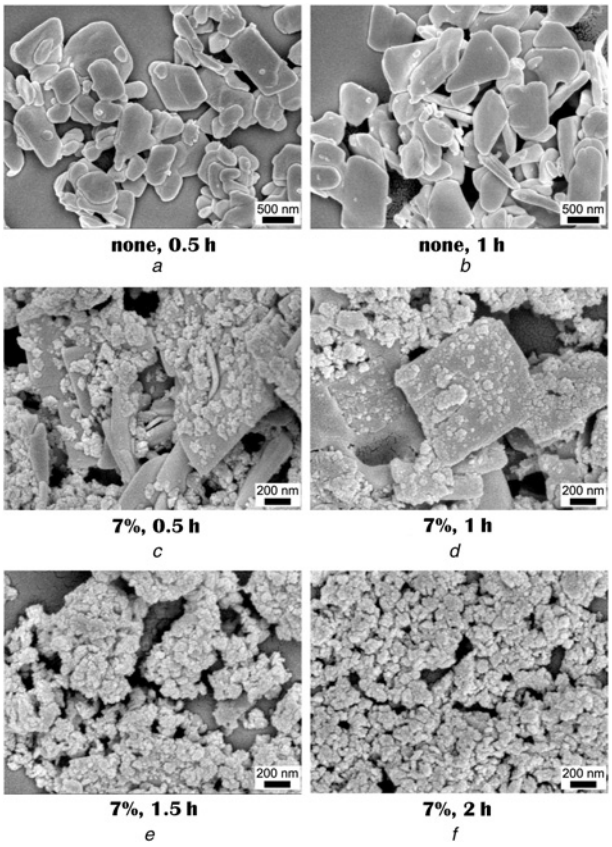


**Fig. 6** *FESEM images of precursors obtained after different reaction time without and with fluorine incorporation*
*a* 0%, 0.5 h
*b* 0%, 1 h
*c* 7%, 0.5 h
*d* 7%, 1 h
*e* 7%, 1.5 h
*f* 7%, 2 h

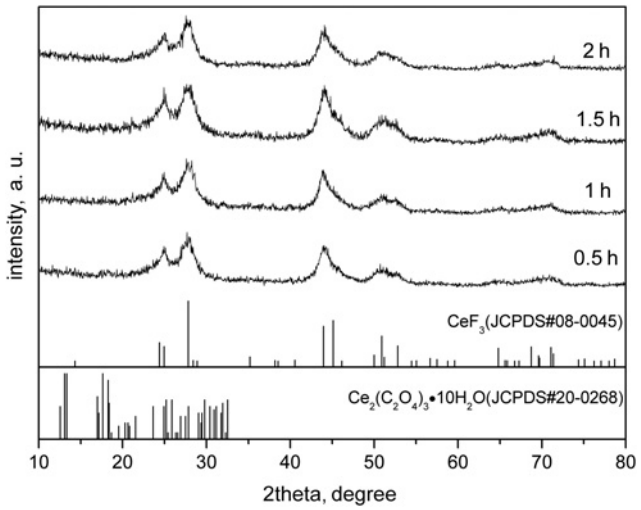


**Fig. 7** *XRD patterns of precursors obtained after different reaction time with 7% fluorine incorporation*

while peaks corresponding to $Ce_2(C_2O_4)_3{\cdot}10H_2O$ phase are not so distinct, indicating that most $Ce_2(C_2O_4)_3{\cdot}10H_2O$ components in the precursors can be amorphous. Meanwhile the profile of four XRD patterns shows no big difference even though the reaction time increases from 0.5 to 2 h, demonstrating that synthesis of




doi: 10.1049/mnl.2017.0303

$CeF_3$ and $Ce_2(C_2O_4)_3{\cdot}10H_2O$ can be completed in a short period. Moreover the intensity of all peaks decreases lightly with the milling time increasing, which may be attributed to increase of amorphous components originated from long-time mechanic-chemical reaction, as evidenced by the vanished weak peaks of $Ce_2(C_2O_4)_3{\cdot}10H_2O$ located at about 18°.

From the results in Fig. 6, it can be concluded easily that the introduction of fluorine in the mechanochemical reactions is the key factor why particles size and morphology change so significantly. Here a possible growth mechanism of the composite powders is discussed. At the beginning of mechanical milling, on account of the stronger electronegativity than $(C_2O_4)^{2-}$ ions, part of $F^-$ ions combine with $Ce^{3+}$ ions, forming fine $CeF_3$ particles, this reaction can be expressed as follows:

$$Ce(NO_3)_3{\cdot}6H_2O + 3NH_4F \rightarrow CeF_3 + 3NH_4NO_3 + 6H_2O \quad (2)$$

meanwhile reaction between cerium nitrate hexahydrate and oxalic acid dihydrate proceeds as (3), forming irregular crystal sheet of $Ce_2(C_2O_4)_3{\cdot}10H_2O$

$$\begin{aligned} &2Ce(NO_3)_3{\cdot}6H_2O + 3H_2C_2O_4 \cdot 2H_2O \\ &\quad \rightarrow Ce_2(C_2O_4)_3{\cdot}10H_2O + 6HNO_3 + 8H_2O \end{aligned} \quad (3)$$

The XRD results in Fig. 7 show that the reactions in (2) and (3) proceed at a rather high rare. Hence a structure composed of smooth $Ce_2(C_2O_4)_3$ crystal sheets with $CeF_3$ particles attaching on their surfaces is obtained. With the milling proceeding, unreacted $F^-$ ions will gradually replace the $(C_2O_4)^{2-}$ ions on the surfaces of cerium oxalate sheets under the strong mechanochemical effect. This reaction can be expressed as follows:

$$\begin{aligned} &Ce_2(C_2O_4)_3{\cdot}10H_2O + 6NH_4F \\ &\quad \rightarrow 2CeF_3 + 3(NH_4)_2C_2O_4 \cdot H_2O + 7H_2O \end{aligned} \quad (4)$$

New $CeF_3$ nucleuses grow up into small spherical protuberances on cerium oxalate's surfaces. As a result, those crystal sheets become much rougher, as shown in Fig. 6*d*. These protuberances constantly increase and grow up, leading to structure looseness of the cerium oxalate crystal sheets. On the other hand, small $CeF_3$ granules formed earlier can play a role of assistant grinding agents. Under the synergy of the above factors, those crystal sheets of cerium oxalate were destroyed little by little under the mechanochemical effect, resulting in small size and uniform morphology, as shown in Figs. 6*e* and *f*. During the subsequent calcination procedure, $Ce_2(C_2O_4)_3{\cdot}10H_2O$ in the precursors is quickly broken down as

$$Ce_2(C_2O_4)_3{\cdot}10H_2O + 2O_2 \rightarrow 2CeO_2 + 6CO_2 + 10H_2O \quad (5)$$

Simultaneously, the amorphous $CeF_3$ in the precursors gains fine crystallinity. Normally, the particles after calcination will inherit the morphology of their precursors, so the final composite product is even nanosized particles with high crystallinity. If no enough fluorine is added in the reaction, cerium oxalate sheets will still maintain big sheet-structure to some extent, resulting in composite powders with sheet shape after calcination, as shown in Figs. 2*b* and *c*.

**4. Conclusion:** $CeO_2/CeF_3$ composite powders were successfully prepared via a simple route of solid-phase mechanochemical method followed by a calcination procedure. The experimental results show that incorporation of 7 wt% fluorine into the starting materials can change the particle morphology from large sheet for pure $CeO_2$ into uniform spherical particles with size of 30–50 nm, and doping excess fluorine will deteriorate various characteristics of products. The composite powder with fluorine doping content of 7 wt% exhibits great suspension stability and relatively high MRR. Their slurry facilitates obtaining smoother surface after CMP, which can be related to the changes of particle morphology and decrease in overall hardness of abrasives.

**5. Acknowledgments:** This work was supported by the Science and Technology Support Program in Sichuan Province (grant no. 2014GZ0090).

## 6 References

[1] Kim S., Saka N., Chun J.H.: 'Pad scratching in chemical-mechanical polishing: the effects of mechanical and tribological properties', *ECS J. Solid State Sci. Technol.*, 2014, **3**, (5), pp. 169–178

[2] Zantye P.B., Kumar A., Sikder A.K.: 'Chemical mechanical planarization for microelectronics applications', *Mater. Sci. Eng. R: Reports*, 2004, **45**, (3-6), pp. 89–220

[3] Luo J.F., Dornfeld D.A.: 'Material removal mechanism in chemical mechanical polishing: theory and modeling', *IEEE Trans. Semicond. Manuf.*, 2001, **14**, (2), pp. 112–133

[4] Nanz G., Camilletti L.E.: 'Modeling of chemical-mechanical polishing: a review', *IEEE Trans. Semicond. Manuf.*, 1995, **8**, (4), pp. 382–389

[5] Wang L., Zhang K., Song Z., *ET AL.*: 'Ceria concentration effect on chemical mechanical polishing of optical glass', *Appl. Surf. Sci.*, 2007, **253**, (11), pp. 4951–4954

[6] Oh M.H., Nho J.S., Cho S.B., *ET AL.*: 'Polishing behaviors of ceria abrasives on silicon dioxide and silicon nitride CMP', *Powder Technol.*, 2011, **206**, (3), pp. 239–245

[7] Oh M.H., Singh R.K., Gupta S., *ET AL.*: 'Polishing behaviors of single crystalline ceria abrasives on silicon dioxide and silicon nitride CMP', *Microelectron. Eng.*, 2010, **87**, (12), pp. 2633–2637

[8] Tsai M.S.: 'Powder synthesis of nano grade cerium oxide via homogenous precipitation and its polishing performance', *Mater. Sci. Eng. B*, 2004, **110**, (2), pp. 132–134

[9] Zhang Z., Yu G., Zhou Y., *ET AL.*: 'A novel strategy for the synthesis of $CeO_2/CeF_3$ composite powders with improved suspension stability and chemical mechanical polishing (CMP) performance', *Arab. J. Sci. Eng.*, 2015, **40**, (10), pp. 2897–2901

[10] Chen A.L., Wang Y.Y., Qin J.W., *ET AL.*: 'Chemical mechanical polishing for $SiO_2$ film using polystyrene@ceria (PS@$CeO_2$) core-shell nanocomposites', *J. Inorg. Organometallic Polym. Mater.*, 2015, **25**, (6), pp. 1407–1413

[11] Yoshida M., Koyama N., Ashizawa T., *ET AL.*: 'A new cerium-based ternary oxide slurry, $CeTi_2O_6$, for chemical-mechanical polishing', *Jpn. J. Appl. Phys.*, 2007, **46**, (3R), p. 977

[12] Lei H., Chu F.L., Xiao B.Q., *ET AL.*: 'Preparation of silica/ceria nano composite abrasive and its CMP behavior on hard disk substrate', *Microelectron. Eng.*, 2010, **87**, (9), pp. 1747–1750

[13] Rajendran A., Takahashi Y., Koyama M., *ET AL.*: 'Tight-binding quantum chemical molecular dynamics simulation of mechano-chemical reactions during chemical–mechanical polishing process of $SiO_2$ surface by $CeO_2$ particle', *Appl. Surf. Sci.*, 2005, **244**, (1), pp. 34–38

[14] Hao S.Y.: 'Ultrafine $CeO_2$: microwave-assisted heating preparation and polishing properties', *Chinese. J. Inorg. Chem.*, 2008, **24**, (6), pp. 1012–1016

[15] Li X.Z., Chen Y., Chen Z.G., *ET AL.*: 'Preparation of $CeO_2$ nanoparticles and their chemical mechanical polishing as abrasives', *Tribology*, 2007, **27**, (1), pp. 1–5